PNAS RESEARCH ARTICLE | IMMUNOLOGY AND INFLAMMATION

RNPS1 inhibits excessive tumor necrosis factor/tumor necrosis factor receptor signaling to support hematopoiesis in mice

Xue Zhong[a,1], Jin Huk Choi[a,1], Sara Hildebrand[a], Sara Ludwig[a], Jianhui Wang[a], Evan Nair-Gill[a], Tzu-Chieh Liao[a], James J. Moresco[a], Aijie Liu[a], Jiexia Quan[a], Qihua Sun[a], Duanwu Zhang[a,2], Xiaoming Zhan[a], Mihwa Choi[a], Xiaohong Li[a], Junmei Wang[b], Thomas Gallagher[a], Eva Marie Y. Moresco[a], and Bruce Beutler[a,3]

Contributed by Bruce Beutler; received January 6, 2022; accepted February 28, 2022; reviewed by Rebecca Buckley and Alain Fischer

Null mutations of spliceosome components or cofactors are homozygous lethal in eukaryotes, but viable hypomorphic mutations provide an opportunity to understand the physiological impact of individual splicing proteins. We describe a viable missense allele (F181I) of *Rnps1* encoding an essential regulator of splicing and nonsense-mediated decay (NMD), identified in a mouse genetic screen for altered immune cell development. Homozygous mice displayed a stem cell–intrinsic defect in hematopoiesis of all lineages due to excessive apoptosis induced by tumor necrosis factor (TNF)–dependent death signaling. Numerous transcript splice variants containing retained introns and skipped exons were detected at elevated frequencies in *Rnps1*$^{F181I/F181I}$ splenic CD8$^+$ T cells and hematopoietic stem cells (HSCs), but NMD appeared normal. Strikingly, *Tnf* knockout rescued all hematopoietic cells to normal or near-normal levels in *Rnps1*$^{F181I/F181I}$ mice and dramatically reduced intron retention in *Rnps1*$^{F181I/F181I}$ CD8$^+$ T cells and HSCs. Thus, RNPS1 is necessary for accurate splicing, without which disinhibited TNF signaling triggers hematopoietic cell death.

TNF | apoptosis | hematopoiesis | splicing

Messenger RNA (mRNA) splicing, both constitutive and alternative, is necessary for the expression of the vast majority of human proteins. Splicing is carried out by the spliceosome ribonucleoprotein complex, consisting of five small nuclear ribonucleoproteins (snRNPs), in a regulated process involving dozens of accessory proteins that modulate spliceosome assembly, 5′ and 3′ splice site selection and pairing, and stabilization of snRNPs at multiple stages of the splicing reaction (1, 2). RNA-binding protein with serine-rich domain 1 (RNPS1) is a splicing regulator initially described as a general activator that promotes splicing of model transcripts in splicing reactions in vitro (3, 4). On the other hand, RNPS1 forms a complex with apoptotic chromatin condensation inducer 1 (ACINUS) and Sin3-associated polypeptide 18 (SAP18), called the apoptosis and splicing-associated protein (ASAP) complex, which inhibits splicing in vitro and promotes apoptosis when the complex is microinjected into HeLa cells, in particular when the complex contains the long isoform of ACINUS (5–9). By association with ASAP or an alternative complex called PSAP (containing Pinin [PNN] rather than ACINUS) and the exon junction complex (EJC), RNPS1 suppresses aberrant usage of cryptic 5′ splice sites (6, 9, 10). RNPS1 also suppresses errors in pre-mRNA splicing (11). RNPS1 was also reported to interact with the EJC and to recruit the UP-Frameshift (UPF) complex to the EJC upon identification of premature termination codons (PTCs) to initiate nonsense-mediated decay (NMD) (12, 13). These findings established the capabilities of RNPS1 for RNA processing and surveillance, but how these functions are utilized in vivo and their physiological importance are unknown.

We identified *Rnps1* in a forward genetic screen for alterations of the relative proportions of immune cells in the peripheral blood of *N*-ethyl-*N*-nitrosourea (ENU)-mutagenized mice. Although null mutations of *Rnps1* were homozygous lethal, an ENU-induced missense allele was viable and caused an immunological phenotype in which development of all hematopoietic lineages was impaired. Here, we describe the immune phenotypes of *Rnps1* mutant mice; the effects of RNPS1 deficiency on the transcriptome and proteome and on splicing; and the surprising discovery that excessive tumor necrosis factor (TNF), a key inflammatory cytokine, is largely responsible for the splicing defects and ensuing hematopoietic cell death in homozygous *Rnps1* mutants.

Results

***Unbalanced*, a Viable Hypomorphic Allele of *Rnps1* Causing Skewing of the CD4:CD8 T Cell Ratio.** Using flow cytometric analysis of peripheral blood, we screened 145,553 third-generation (G3) mice derived from 4,145 pedigrees bearing 226,041 nonsynonymous mutations

Significance

Messenger RNA (mRNA) splicing is fundamental to protein expression in mammals. Homozygous deletion of single protein components of the splicing machinery or its regulatory factors is embryonic lethal. However, through forward genetic screening in mice, we identified a viable hypomorphic missense mutation of the splicing regulator RNPS1. Homozygous mutant mice displayed altered immune cell development due to excessive tumor necrosis factor (TNF)–dependent immune cell apoptosis. Splicing was impaired in CD8$^+$ T cells and hematopoietic stem cells from RNPS1 mutant mice. TNF knockout rescued hematopoiesis and dramatically reduced splicing defects in RNPS1 hematopoietic cells, demonstrating a surprising link between elevated TNF and defects in splicing caused by RNPS1 deficiency.

Author contributions: X. Zhong, J.H.C., and B.B. designed research; X. Zhong, J.H.C., S.L., Jianhui Wang, E.N.-G., T.C.L., J.J.M., A.L., J.Q., Q.S., D.Z., X. Zhan, M.C., X.L., and Junmei Wang performed research; X. Zhong, J.H.C., and S.H. analyzed data; and X. Zhong, E.N.-G., T.G., E.M.Y.M., and B.B. wrote the paper.

Reviewers: R.B., Duke University; and A.F., Institut Imagine Institut des Maladies Genetiques.

The authors declare no competing interest.

[1]X. Zhong and J.H.C. contributed equally to this work.

[2]Present address: Children's Hospital of Fudan University and Institutes of Biomedical Sciences, Fudan University, Shanghai 200032, China.

[3]To whom correspondence may be addressed. Email: Bruce.Beutler@UTSouthwestern.edu.

This article contains supporting information online at http://www.pnas.org/lookup/suppl/doi:10.1073/pnas.2200128119/-/DCSupplemental.

Published April 28, 2022.

within coding regions or splice junctions of 21,118 genes. Overall, we tested 52.4% of all protein-encoding genes in the genome, wherein one or more truly damaging or destructive variant alleles (14) were examined for phenotypic effects three times or more in the homozygous state. Several mice from a single pedigree showed an increased ratio of $CD4^+$ to $CD8^+$ T cells in the blood (Fig. 1 *A* and *B*). This recessive phenotype, named *unbalanced,* mapped to a plus-sense T to A transversion at chromosome 17:24422168 in the coding region of *Rnps1* (Fig. 1*A*). The point mutation caused a phenylalanine to isoleucine substitution at position 181 of the encoded protein, located in the RNA recognition motif (Fig. 1*C*). RNPS1 orthologs from humans, mice, and cattle share 100% amino acid sequence identity (*SI Appendix*, Fig. S1), and the F181 residue is conserved in all species we examined, including representative vertebrates, invertebrates, and *Schizosaccharomyces pombe* (*SI Appendix*, Fig. S1). Thus, we consider it likely that RNPS1 has similar functions in all eukaryotes and that F181 is important for some of these functions.

We attempted to verify the *Rnps1* mutation as causative of the *unbalanced* phenotype using a CRISPR-Cas9 knockout strategy. We were unable to obtain any pups homozygous for *Rnps1* null alleles, leading us to conclude that complete ablation of this gene is lethal prior to weaning age (Table 1). Therefore, we used CRISPR-Cas9 to engineer a germline replacement of the T to A point mutation found in *unbalanced* mice. Mice homozygous for the CRISPR-Cas9–generated *unbalanced* allele ($Rnsp1^{F181I/F181I}$) showed an increased $CD4^+$ to $CD8^+$ T cell ratio identical to the mice harboring the original ENU-induced allele (Fig. 1*D*). Compound heterozygotes ($Rnps1^{F181I/-}$) from crosses of $Rnps1^{F181I/+}$ and $Rnps1^{+/-}$ mice were also unable to survive to weaning age (Table 1). Mating $Rnps1^{F181I/+}$ mice did not produce the expected Mendelian ratio of $Rnps1^{F181/181}$ progeny: $Rnps1^{+/+}$, $Rnps1^{F181I/+}$, $Rnps1^{F181I/F181I}$ represented 29.7%, 63.1%, and 7.2% of the offspring, respectively (Table 1). These findings demonstrate that although compatible with life, homozygosity for the F181I allele of *Rnps1* caused reduced viability. However, $RNPS1^{F181I}$ protein was expressed at normal levels in all tissues examined from homozygotes (Fig. 1*E*). $Rnps1^{F181I/F181I}$ mice were ∼30% smaller than their wild-type (WT) littermates (*SI Appendix*, Fig. S2*A*), displayed elevated susceptibility to dextran sodium sulfate–induced colitis (*SI Appendix*, Fig. S2*B*), had no obvious external deformities, and appeared to live a normal life span.

Pancytopenia and Impaired Hematopoietic Stem Cell (HSC) Development in $Rnps1^{F181I/F181I}$ Mice. We subjected $Rnps1^{F181I/F181I}$ mice to the comprehensive immune cell population and immune function analyses routinely applied to all mutant strains identified with a flow cytometry phenotype. These include assays for infection with mouse cytomegalovirus (MCMV) (Fig. 2 *A* and *B*), in vivo natural killer (NK) cell and cytotoxic T lymphocyte (CTL) cytolytic activity (Fig. 2 *C–E*), and T cell–dependent antibody responses to immunization with alum-precipitated ovalbumin (alum-OVA) (*SI Appendix*, Fig. S2*M*), all of which were altered in $Rnps1^{F181I/F181I}$ mice. Although we found that $Rnps1^{F181I/F181I}$ mice also exhibited impaired B cell development (*SI Appendix*, Fig. S2 *C–K*) and function (*SI Appendix*, Fig. S2*L*), we focus here on the T cell and HSC phenotypes in $Rnps1^{F181I/F181I}$ mice, as described below.

Complete blood count testing indicated that $Rnps1^{F181I/F181I}$ mice were pancytopenic (Fig. 2*F*). We therefore tested whether deficiencies extended to HSC and progenitor cell populations. We found ∼50% reductions in the frequencies of Lin^-c-$kit^+Sca\text{-}1^+$ (LSK) cells, which contain HSC, and common lymphoid progenitors (CLPs), gated from Lin^-c-$kit^{low}Sca\text{-}1^{low}$ cells, in $Rnps1^{F181I/F181I}$ bone marrow relative to WT bone

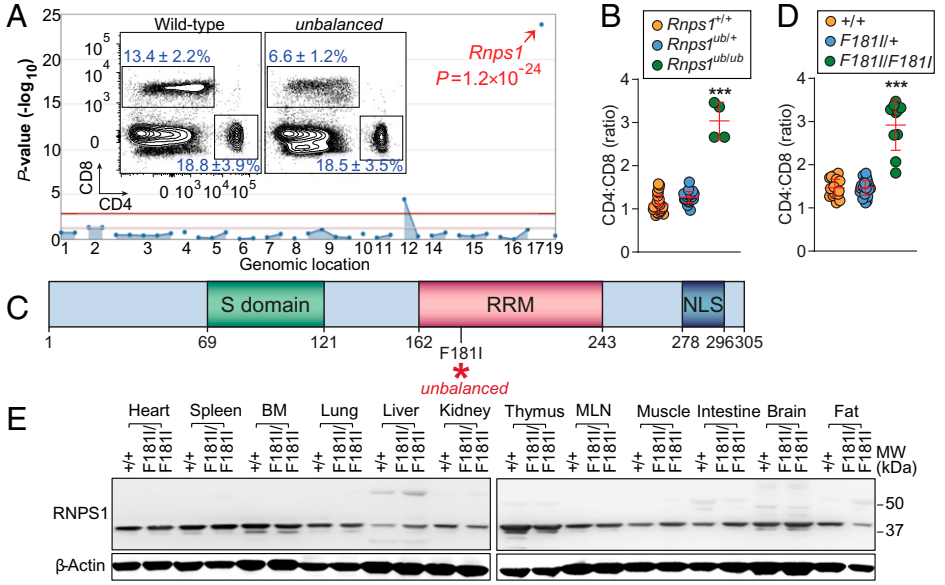

Fig. 1. *Unbalanced*, a viable hypomorphic allele of *Rnps1* causing skewing of the CD4:CD8 T cell ratio. (*A*) Manhattan plot. $-\text{Log}_{10}$ *P* values plotted versus the chromosomal positions of mutations identified in the Generation 1 (G1) founder of the affected pedigree. The *Insets* show representative flow cytometry plots of $CD4^+$ and $CD8^+$ peripheral blood lymphocytes in WT and *unbalanced* mice. Numbers adjacent to outlined regions indicate percent cells in each expressed as mean ± SD (n = 4 *ub/ub* mice, 27 WT littermates). (*B*) The ratio of $CD4^+$ and $CD8^+$ peripheral blood T cells from G3 descendants of a single ENU-mutagenized male mouse, with $^{+/+}$, *+/ub*, or *ub/ub* genotypes for *Rnps1* (n = 4 to 27 mice/genotype). (*C*) RNPS1 topology. Schematic of RNPS1 domains and the substitution of phenylalanine to isoleucine at position 181 of total 305 amino acids. Numbers indicate amino acid positions. S domain, serine-rich (S) domain; RRM, RNA recognition motif; NLS, nuclear localization signal. (*D*) The ratio of $CD4^+$ and $CD8^+$ peripheral blood T cells from 10-wk-old WT ($^{+/+}$), $Rnps1^{F181I/+}$ (*F181I/*$^+$), and $Rnps1^{F181I/F181I}$ (*F181I/F181I*) mice generated by the CRISPR-Cas9 system (n = 10 to 35 mice/genotype). (*E*) Immunoblot analysis of RNPS1 in various tissues from WT ($^{+/+}$) or $Rnps1^{F181I/F181I}$ (*F181I/F181I*) mice. BM, bone marrow; MLN, mesenteric lymph node; MW, molecular weight. Data are representative of one experiment (*A, B, D,* and *E*). Data points represent individual mice. Error bars indicate SD. *P* values were determined by one-way analysis of variance (ANOVA) with Dunnett's multiple comparisons (*B* and *D*). ***$P < 0.001$.

Table 1. Offspring from crosses of *Rnps1* mutant mice

Cross	Offspring: Genotype	Number	Frequency, % Actual	Frequency, % Expected	*P*
$Rnps1^{+/-} \times Rnps1^{+/-}$	+/−	64	66.7	50	1.125×10^{-7}
	+/+	32	33.3	25	
	−/−	0	0	25	
$Rnps1^{+/F181I} \times Rnps1^{+/F181I}$	F181I/+	591	63.1	50	7.88×10^{-25}
	+/+	278	29.7	25	
	F181I/F181I	67	7.2	25	
$Rnps1^{+/F181I} \times Rnps1^{+/-}$	F181I/+	41	32.0	25	1.46×10^{-9}
	+/+	48	37.5	25	
	+/−	39	30.4	25	
	F181/−	0	0	25	
$Rnps1^{F181I/F181I}Tnf^{-/-} \times Rnps1^{+/F181I}Tnf^{-/-}$	F181I/+;$Tnf^{-/-}$	51	56.0	50	0.2301
	F181I/F181I;$Tnf^{-/-}$	40	44.0	50	

A χ^2 test with the appropriate degrees of freedom was used to calculate *P* values.

marrow (Fig. 2 *G–I* and *SI Appendix*, Fig. S3). $Rnps1^{F181I/F181I}$ mice had decreased frequencies of multipotent progenitors, lymphoid-primed multipotent progenitors, common myeloid progenitors, and megakaryocyte-erythroid progenitors and elevated proportions of short-term HSC and granulocyte-macrophage progenitors (Fig. 2*I* and *SI Appendix*, Fig. S3). Total numbers per femur of all the populations were diminished in $Rnps1^{F181I/F181I}$ mice compared to WT littermates (Fig. 2*J*).

To determine whether the hematopoietic defects were intrinsic to $Rnps1^{F181I/F181I}$ cells, mixed bone marrow chimeras were generated by reconstituting lethally irradiated $Rag2^{-/-}$ recipients with a 1:1 mixture of $Rnps1^{F181I/F181I}$ (CD45.2) HSCs (Fig. 2*K*) or their littermate $Rnps1^{+/+}$ (CD45.2) HSCs (Fig. 2*L*) and WT (CD45.1) HSCs (LSK population), sorted from bone marrow cells (*SI Appendix*, Fig. S4). At 12 wk after transplant, $Rnps1^{F181I/F181I}$ cells were at a striking disadvantage compared to WT HSCs in repopulating the peripheral blood mononuclear cell (PBMC) compartment (CD45.2) (Fig. 2 *K* and *L*). HSCs from $Rnps1^{F181I/F181I}$ donors were unable to repopulate $CD8^+$ T cells in the peripheral blood of recipients as efficiently as cells derived from WT donors (Fig. 2*M*), resulting in an elevated $CD4^+$ to $CD8^+$ T cell ratio for $Rnps1^{F181I/F181I}$ donor-derived T cells (Fig. 2 *N* and *O*). These results indicate a cell-intrinsic defect in $Rnps1^{F181I/F181I}$ HSC impaired early immune cell development. However, the F181I substitution in RNPS1 caused no apparent lymphoid and myeloid commitment bias effects.

Impaired T Cell Development and Survival in *Rnps1* Mutant Mice. Reduced frequencies of total T cells and $CD8^+$ T cells (Fig. 3 *A* and *B*) were detected in the blood of $Rnps1^{F181I/F181I}$ mice compared with WT littermates; the frequency of $CD4^+$ T cells was similar in $Rnps1^{F181I/F181I}$ and WT mice (*SI Appendix*, Fig. S5*A*). Compared to WT littermates, $Rnps1^{F181I/F181I}$ mice had reduced splenic $CD8^+$ T cells but similar numbers of splenic $CD4^+$ T cells (Fig. 3*C*). These data, together with the findings from mixed bone marrow transplantation (Fig. 2 *M–O*), suggested a more pronounced effect of the mutation on $CD8^+$ than on $CD4^+$ T cells. Thymocyte numbers were reduced (Fig. 3*C*), and their development was abnormal in $Rnps1^{F181I/F181I}$ mice (*SI Appendix*, Fig. S5 *B–E* and Supplementary Text). $Rnps1^{F181I/F181I}$ thymocytes expressed elevated amounts of CD44, and mature peripheral $CD8^+$ T cells contained a high frequency of effector memory T cells, suggesting they were abnormally activated (Fig. 3 *D* and *E*). There were no changes in the frequencies of naive, central memory, or effector memory T cells in the $CD4^+$ T cell population or in the frequencies of naive or central memory T cells in the $CD8^+$ T cell population found in the blood of $Rnps1^{F181I/F181I}$ mice compared to WT littermates. We observed ~1.5 times more apoptotic $Rnps1^{F181I/F181I}$ thymocytes than WT thymocytes at all developmental stages and ~1.8 times more apoptotic $CD4^+$ and $CD8^+$ T cells in the spleens of $Rnps1^{F181I/F181I}$ mice relative to WT mice, suggesting defective maintenance of the peripheral T cell pool (Fig. 3*F*). Analyses of homeostatic and antigen-induced T cell proliferation showed that $Rnps1^{F181I/F181I}$ T cells proliferated normally (Fig. 3 *G–N*) but contained a larger proportion of apoptotic cells relative to WT T cells (*SI Appendix*, Fig. S5 *F–H* and Supplementary Text). These data indicate that $Rnps1^{F181I/F181I}$ T cells exhibited an intrinsic survival defect under lymphocyte replete conditions that worsened in response to homeostatic or antigen-specific expansion signals.

***Rnps1*$^{F181I/F181I}$ T Cell and HSC Developmental Defects Caused by Excessive TNF-Induced Death Signaling.** Two major molecular pathways mediate apoptosis in immune cells: i) The cell-extrinsic pathway is initiated upon the binding of death ligands such as Fas and TNF to death receptors on the cell surface, and ii) the cell-intrinsic pathway is initiated upon procaspase-9 cleavage and culminates in cleavage of lamin A/C. We examined these apoptotic pathways in isolated splenic $CD8^+$ T cells. We found that under baseline (unstimulated) conditions, the activation of both the extrinsic and the intrinsic apoptotic pathways in $Rnps1^{F181I/F181I}$ $CD8^+$ T cells was similar to that observed in WT cells (Fig. 4*A*). Activation of the extrinsic apoptotic pathway using Fas ligand (FasL) resulted in similar levels of caspase cleavage in $Rnps1^{F181I/F181I}$ and WT $CD8^+$ T cells (Fig. 4*A*). We also found that mutation of Fas did not rescue the T cell deficiency in $Rnps1^{F181I/F181I}$ mice (Fig. 4 *B* and *C*). In contrast, stimulation with TNF triggered higher levels of cleaved caspase-9, cleaved caspase-8, cleaved caspase-7, cleaved caspase-3, cleaved ACINUS, and cleaved poly (ADP-ribose) polymerase 1 (PARP), but not cleaved caspase-6, in $Rnps1^{F181I/F181I}$ $CD8^+$ T cells compared to WT $CD8^+$ T cells (Fig. 4*D*). These effects were not observed in $Rnps1^{F181I/F181I}$ $CD4^+$ T cells (*SI Appendix*, Fig. S6).

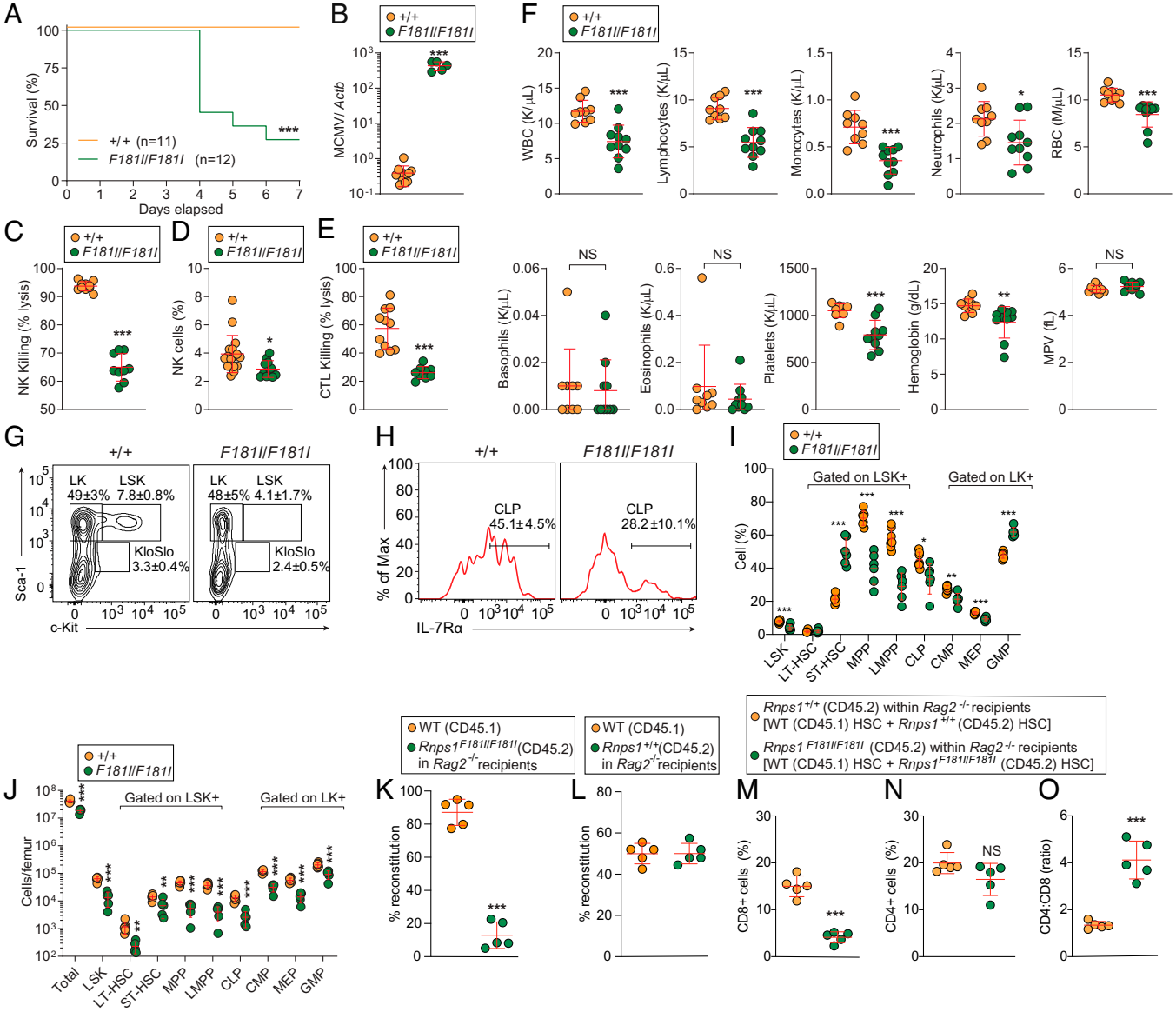

Fig. 2. Pancytopenia and impaired HSC development in *F181I/F181I* mice. (*A*) Survival curves after MCMV infection (n = 11 or 12 mice per genotype). The experiment was concluded after 7 d. (*B*) Viral DNA copies in spleen 5 d after infection with 1.5 × 10^5 PFUs MCMV Smith strain (n = 5 to 12 mice per genotype) *Actb*, β-*actin* gene. (*C*) NK cell cytotoxicity against MHC class I–deficient ($\beta 2m^{-/-}$) target cells (n = 9 or 10 mice/genotype). (*D*) Frequency of NK cells in the peripheral blood from 10-wk-old mice (n = 10 to 17 mice/genotype). (*E*) Quantitative analysis of the OVA-specific cytotoxic T cell–killing response in littermate mice immunized with alum-OVA (n = 9 to 11 mice/genotype). (*F*) Complete blood count testing. WBCs, lymphocytes, monocytes, neutrophils, RBCs, basophils, eosinophils, platelets, hemoglobin, and mean platelet volume (MPV) in 8-wk-old littermates (n = 9 or 10 mice/genotype). (*G* and *H*) Representative flow cytometry plots of Lineage-marker negative (Lin^-) populations (*G*) and CLP (*H*) from littermates. Numbers adjacent to outlined regions (*G* and *H*) indicate percentage of cells in each expressed as mean ± SD (n = 7 WT mice, 5 *F181I/F181I* littermates). (*I* and *J*) Frequency (*I*) and numbers (*J*) of HSC and progenitor populations in the bone marrow of 10-wk-old littermates (n = 5 to 7 mice/genotype). (*K* and *L*) Repopulation of total PBMCs 12 wk after the reconstitution of lethally irradiated $Rag2^{-/-}$ recipients with a 1:1 mixture of *F181I/F181I* (*K*) or $^{+/+}$ (*L*) HSCs (CD45.2) and congenic WT HSCs (C57BL/6J; CD45.1). (*M*–*O*) Repopulation of CD45.2 ($^{+/+}$ or *F181I/F181I*) $CD8^+$ T cells (*M*), $CD4^+$ T cells (*N*), and ratio of $CD4^+$ and $CD8^+$ T cells (*O*) in the peripheral blood 12 wk after the reconstitution of lethally irradiated $Rag2^{-/-}$ recipients with a 1:1 mixture of $^{+/+}$ or *F181I/F181I* HSCs (CD45.2) and congenic WT HSCs (C57BL/6J; CD45.1). Donor chimerism levels in the peripheral blood were assessed using congenic CD45 markers (n = 5 recipients/group). Data are representative of one experiment (*A*–*E* and *K*–*O*) or two independent experiments (*F*–*J*). Data points represent individual mice. Error bars indicate SD. *P* values were determined by Student *t* test (*B*–*F* and *I*–*O*). Survival curve *P* value ($^{+/+}$ versus *F181I/F181I*) in *A* was calculated by Log-rank (Mantel-Cox) test. Log_{10} of viral titers in *B* was used for *P* value calculation. *$P < 0.05$; **$P < 0.01$; ***$P < 0.001$; NS, not significant. $^{+/+}$ indicates WT and *F181I/F181I* indicates the $Rnps1^{F181I/F181I}$ genotype. LSK, $Lin^-c\text{-}Kit^+$ $Sca\text{-}1^+$; LK, Lin^- $c\text{-}Kit^+$ $Sca\text{-}1^-$; LT-HSC, long-term hematopoietic stem cell; ST-HSC, short-term hematopoietic stem cell; MPP, multipotent progenitor cell; LMPP, lymphoid-primed multipotent progenitor; MEP, megakaryocyte–erythroid progenitor; CMP, common myeloid progenitor; GMP, granulocyte-macrophage progenitor; KloSlo, $Lin^-c\text{-}kit^{low}Sca\text{-}1^{low}$; IL, interleukin; Max, maximum.

Strikingly, homozygosity for a null allele of *Tnf* rescued the reduced numbers of white blood cells (WBCs), lymphocytes, monocytes, neutrophils, and platelets in $Rnps1^{F181I/F181I}$ mice to WT levels, with only red blood cells and $CD8^+$ T cells not recovering fully (Fig. 4 *E*–*M* and *SI Appendix*, Fig. S7*A*). $Rnps1^{F181I/F181I}$;$Tnf^{-/-}$ mice also showed normal CD4:CD8 T cell ratios (Fig. 4*K*), although the frequency of circulating $CD8^+$ T cells was slightly reduced compared to that in WT mice (Fig. 4 *L* and *M*). Moreover, all HSC and progenitor cell populations were rescued to WT levels in $Rnps1^{F181I/F181I}$; $Tnf^{-/-}$ mice (Fig. 4*N*). These data suggest that $Rnps1^{F181I/F181I}$ cells are killed by TNF stimulation, which induces enhanced activation of the cell-extrinsic apoptosis pathway, leading to the death of HSCs and T cells.

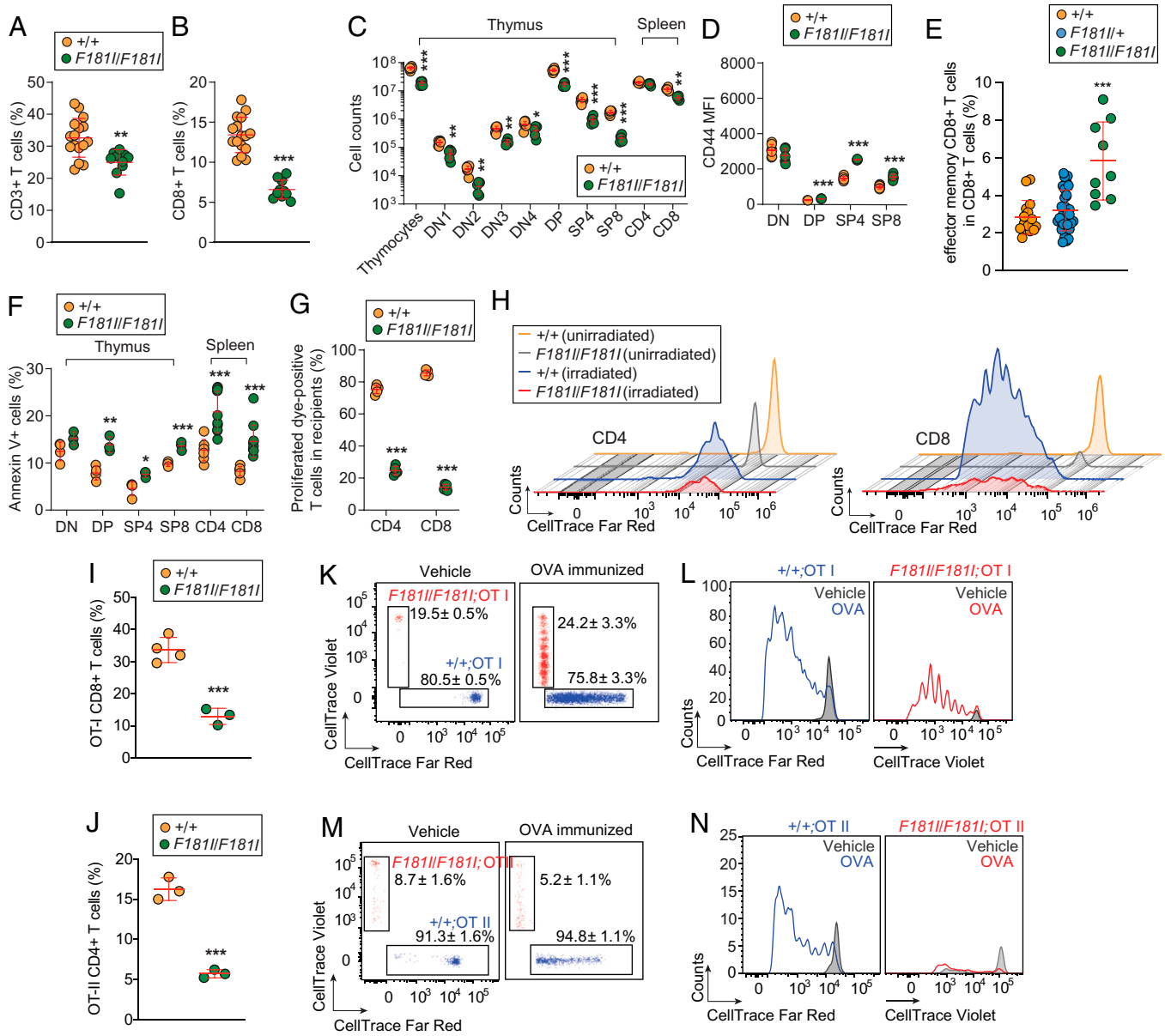

Fig. 3. Impaired T cell development and survival in *F181I/F181I* mice. (*A* and *B*) Frequency of T cells (*A*) and CD8$^+$ T cells (*B*) in the peripheral blood from 10-wk-old mice (n = 10 to 17 mice/genotype). (*C*) Numbers of each thymocyte or splenic T cell population in 10-wk-old littermates (n = 5 to 7 mice/genotype). (*D*) Flow cytometry analysis of CD44 expression on thymic T cells in 10-wk-old littermates (n = 10 to 17 mice/genotype). (*E*) Frequency of effector memory CD8$^+$ T cells in peripheral blood CD8$^+$ T cells from 10-wk-old littermates (n = 9 to 34 mice/genotype). (*F*) Annexin V staining of thymocyte subsets and CD4$^+$ or CD8$^+$ T cells in spleen obtained from 10- to 12-wk-old littermates (n = 5 to 11 mice per genotype). (*G* and *H*) Impaired homeostatic expansion of *F181I/F181I* T cells. An equal mixture of CellTrace Far Red–labeled splenic pan-T cells from CD45.1 ($^{+/+}$) or CD45.2 (*F181I/F181I*) mice isolated from spleen were adoptively transferred into sublethally irradiated (8.5 Gy) WT hosts. Frequency of proliferated dye-positive T cells (*G*) and representative flow cytometric histograms of Far Red dilution in CD4$^+$ or CD8$^+$ T cells (*H*) from spleen of sublethally irradiated or unirradiated WT recipients 7 d after transfer (n = 5 recipients/group). (*I* and *J*) Frequency of OT-I CD8$^+$ T cells (*I*) and OT-II CD4$^+$ T cells (*J*) in the peripheral blood from 10-wk-old WT and *F181I/F181I* OT-I or OT-II mice (n = 3 or 4 mice/genotype). (*K–N*) Impaired antigen-specific expansion of *F181I/F181I* T cells. A 1:1 mixture of CellTrace Violet–labeled *F181I/F181I* (CD45.2) and Far Red–stained WT (CD45.2) OT-I (*K* and *L*) or OT-II cells (*M* and *N*) were adoptively transferred into WT hosts (C57BL/6; CD45.1). Representative FACS scatter plots (OT-I, *K*; OT-II, *M*) and histograms of CellTrace Violet or Far Red dilution (OT-I, *L*; OT-II, *N*) in WT or *F181I/F181I* cells harvested from spleens of WT (C57BL/6J; CD45.1) hosts 48 h after injection of soluble OVA or sterile PBS (vehicle) as a control. Numbers adjacent to outlined regions (*K* and *M*) indicate percent cells in each expressed as means ± SD (n = 5 recipients/OT-I group, 6 recipients/OT-II group). Data are representative of one experiment (*A, B,* and *E*) or two independent experiments (*C, D, F–N*). Data points represent individual mice. Error bars indicate SD. *P* values were determined by Student *t* test (*A–D, F, G, I, J*) and one-way analysis of variance (ANOVA) with Dunnett's multiple comparisons (*E*). *P < 0.05; **P < 0.01; ***P < 0.001. $^{+/+}$ indicates WT and *F181I/F181I* indicates the *Rnps1*$^{F181I/F181I}$ genotype. DN, double-negative; DP, double-positive; SP, single-positive; MFI, mean fluorescence intensity.

Mating *Rnps1*$^{F181I/F181I}$;*Tnf*$^{-/-}$ (male) with *Rnps1*$^{+/F181I}$;*Tnf*$^{-/-}$ (female) mice produced roughly the expected Mendelian ratios of progeny with *Rnps1*$^{+/F181I}$;*Tnf*$^{-/-}$ (expected 50%; actual 56%) and *Rnps1*$^{F181I/F181I}$;*Tnf*$^{-/-}$ (expected 50%; actual 44%) genotypes (Table 1). This finding demonstrates that a null allele of *Tnf* rescues the reduced viability caused by homozygosity for the *Rnps1*^{F181I} allele.

We detected elevated serum TNF concentrations in *Rnps1*$^{F181I/F181I}$ mice compared to WT littermates (Fig. 4*O*), and T cell stimulation with phorbol myristate acetate (PMA)/ionomycin induced TNF expression by approximately twofold more *Rnps1*$^{F181I/F181I}$ T cells than WT T cells, while interferon (IFN)-γ–expressing cells were comparable (Fig. 4 *P* and *Q*). Lethally irradiated *Rag2*$^{-/-}$ mice reconstituted with a 1:1

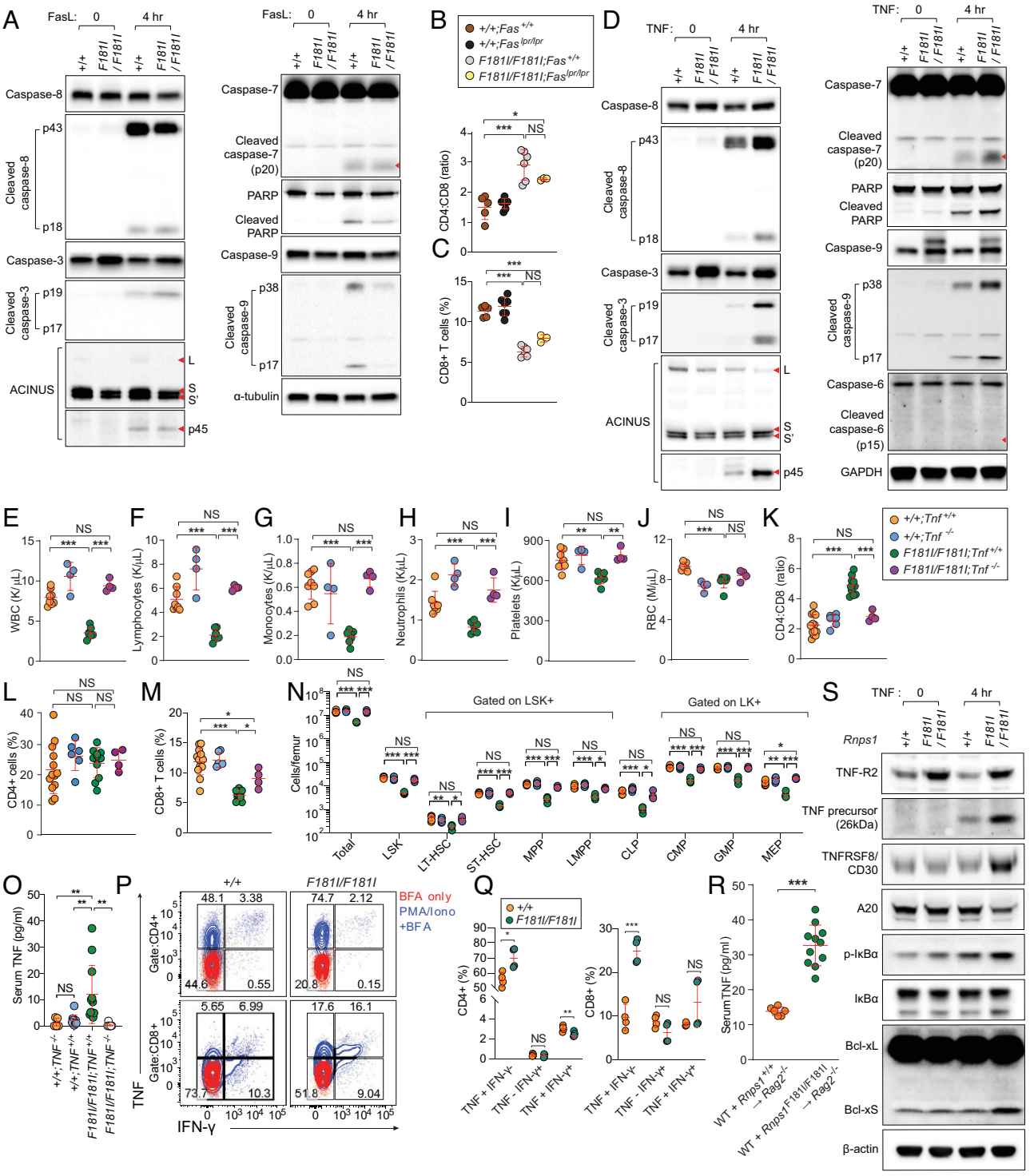

Fig. 4. *F181I/F181I* T cell and HSC developmental defects caused by excessive TNF-induced death signaling. (*A* and *D*) Immunoblot analysis of caspase processing or cleavage of ACINUS and PARP in lysates of pooled splenic CD8$^+$ T cells from WT mice or *F181I/F181I* littermates upon FasL (25 ng/mL; *A*) or TNF (50 ng/mL; *D*) stimulation for 4 h or left untreated. Long- (L) and short- (S or S′) isoforms of ACINUS. (*B* and *C*) The ratio of CD4$^+$ and CD8$^+$ T cells (*B*) and frequency of CD8$^+$ T cells (*C*) in the peripheral blood from 10-wk-old mice (n = 3 to 7 mice/genotype). (*E–J*) Complete blood count testing. WBCs (*E*), lymphocytes (*F*), monocytes (*G*), neutrophils (*H*), platelets (*I*), and RBCs (*J*) in 10-wk-old mice (n = 4 to 8 mice/genotype). (*K–M*) The ratio of CD4$^+$ and CD8$^+$ T cells (*K*) and frequency of CD4$^+$ T cells (*L*) and CD8$^+$ T cells (*M*) in the peripheral blood from 10-wk-old mice (n = 4 to 13 mice/genotype). (*N*) Quantitative analysis of HSC and progenitor populations in the bone marrow of 10-wk-old mice (n = 3 to 6 mice/genotype). (*O*) Serum TNF production in 12- to 14-wk-old mice (n = 3 to 21 mice/genotype). (*P* and *Q*) Representative flow cytometry plots (*P*) and quantitation (*Q*) of TNF$^+$ or/and IFN-γ^+ splenic T cells from littermate mice in response to brefeldin A (BFA) alone or combined with PMA/ionomycin (Iono) stimulation in vitro (n = 4 mice/genotype). Numbers adjacent to outlined regions indicate percent cells in each. (*R*) Serum TNF levels 12 wk after the reconstitution of lethally irradiated *Rag2*$^{-/-}$ recipients with a 1:1 mixture of *Rnps1*$^{+/+}$ or *Rnps1*$^{F181I/F181I}$ bone marrow (CD45.2) cells and congenic WT bone marrow (C57BL/6J; CD45.1) (n = 6 to 11 recipients/group). (*S*) Immunoblot analysis of TNF-R2, TNF precursor, TNFRSF8/CD30, A20, phospho-IκBα (p-IκBα), IκBα, BCL-X, and β-actin in lysates of total splenic CD8$^+$ T cells from WT mice or *F181I/F181I* littermates upon TNF (50 ng/mL) stimulation for 4 h or left untreated. Data are from one experiment (*A–C, O, R*) or are representative of two independent experiments (*D–N, P, Q, S*). Data points represent individual mice. Error bars indicate SD. *P* values were determined by one-way analysis of variance (ANOVA) with Dunnett's multiple comparisons (*B, C, E–O*) or Student *t* test (*Q* and *R*). *P < 0.05; **P < 0.01; ***P < 0.001; NS, not significant. $^{+/+}$ indicates WT and *F181I/F181I* indicates the *Rnps1*$^{F181I/F181I}$ genotype. LSK, Lin$^-$ c-Kit$^+$ Sca-1$^+$; LK, Lin$^-$ c-Kit$^+$ Sca1$^-$; LT-HSC, long-term hematopoietic stem cell; ST-HSC, short-term hematopoietic stem cell; MPP, multipotent progenitor cell; LMPP, lymphoid-primed multipotent progenitor; MEP, megakaryocyte–erythroid progenitor; CMP, common myeloid progenitor; GMP, granulocyte-macrophage progenitor; GAPDH, glyceraldehyde-3-phosphate dehydrogenase.

mixture of *Rnps1*$^{F181I/F181I}$ (CD45.2) and WT (CD45.1) bone marrow showed an approximately twofold increase in serum TNF concentration compared to mice reconstituted with a 1:1 mixture of *Rnps1*$^{+/+}$ (CD45.2) and WT (CD45.1) bone marrow (Fig. 4*R*). WT CD45.1 bone marrow cells displayed normal hematopoiesis in the mixed chimeras that received WT and *Rnps1*$^{F181I/F181I}$ bone marrow cells (*SI Appendix*, Fig. S7*B*), indicating that the elevated TNF in these mice was by itself insufficient to significantly impair hematopoiesis. These data suggest that excess TNF is generated predominantly by *Rnps1*$^{F181I/F181I}$ cells of the hematopoietic lineage in vivo and that autocrine or paracrine TNF stimulation of *Rnps1*$^{F181I/F181I}$ cells is responsible for their impaired survival and development. Notably, except for elevated IFN-α produced in response to double-stranded DNA (dsDNA) treatment, innate immune responses to all tested stimuli were normal in *Rnps1*$^{F181I/F181I}$ peritoneal macrophages (*SI Appendix*, Fig. S7*C*). Similar IFN-α concentrations were detected in serum from *Rnps1*$^{F181I/F181I}$ mice and WT littermates (*SI Appendix*, Fig. S7*D*).

In addition to the caspase-mediated apoptosis pathway, TNF activates a nuclear factor κB (NF-κB)–mediated survival pathway (15, 16). We examined both death receptor signaling and NF-κB signaling events in *Rnps1*$^{F181I/F181I}$ splenic CD8$^+$ T cells (Fig. 4*S*). Without stimulation, several TNF and NF-κB signaling components in *Rnps1*$^{F181I/F181I}$ CD8$^+$ T cells appeared to have equivalent expression, with a notable exception of TNF-R2, which was up-regulated compared to WT (Fig. 4*S*). After challenge with TNF, *Rnps1*$^{F181I/F181I}$ CD8$^+$ T cells showed increased levels of TNF-R2, TNFRSF8, phospho-IκBα, phospho-p65, and BCL-XS, but expression comparable to WT CD8$^+$ T cells of TNF-R1, TRADD, MYD88, and NF-κB2 (Fig. 4*S* and *SI Appendix*, Fig. S7*E*). A20, a negative regulator of NF-κB signaling and TNF-mediated apoptosis (17), was reduced in TNF-stimulated *Rnps1*$^{F181I/F181I}$ T cells compared to WT T cells (Fig. 4*S*). As expected, TNF precursor protein was also elevated in *Rnps1*$^{F181I/F181I}$ CD8$^+$ T cells (Fig. 4*S*). Similar phenotypes were observed in *Rnps1* knockout (*Rnps1*-KO) EL4 cells (a T cell line) (*SI Appendix*, Fig. S8 and Supplementary Text).

Collectively, our data indicate that RNPS1 deficiency resulted in excessive hematopoietic cell–dependent TNF production and, by virtue of elevated receptor expression, hypersensitivity to TNF resulting in increased apoptosis and NF-κB signaling.

Elevated Intron Retention and Exon Skipping and Splicing Alterations Secondary to TNF in *Rnps1*$^{F181/F181I}$ Cells. We sought to understand the mechanistic connection between RNPS1, a known splicing regulator, and TNF, a regulator of inflammatory signaling and apoptosis produced by and acting upon T cells and innate immune cells (18–20). We examined the interactions between RNPS1^{WT} or RNPS1^{F181I} with components of the ASAP complex (RNPS1, ACINUS, and SAP18), PSAP complex, EJC, and NMD complex by coimmunoprecipitation (Co-IP) from HEK293T cell lysates. The F181I mutation did not affect complex formation of RNPS1 with UPF2, UPF3a (NMD complex), EIF4A3, Y14, or MLN51 (EJC) in HEK293T cells (Fig. 5*A*). However, the mutation reduced the interaction of human influenza hemagglutinin (HA)-tagged RNPS1 with SAP18 and with PNN, although RNPS1^{F181I} and RNPS1^{WT} immunoprecipitated similar amounts of ACINUS (Fig. 5*A*). These findings are consistent with the binding free energies ($\Delta G_{F181I\text{-}WT}$) of the PSAP and ASAP complexes containing either RNPS1^{F181I} or RNPS1^{WT} (*SI Appendix*, Table S1), calculated using the molecular mechanics/Poisson-Boltzmann surface area (MM/PBSA)-weighted solvent-accessible surface area (WSAS) based on molecular dynamic (MD) simulations (*Materials and Methods*). The MD structure of the PSAP complex (6) suggested the loss of a stabilizing β-sheet in the RNPS1^{F181I}-containing structure in comparison to the RNPS1^{WT}-containing structure (*SI Appendix*, Fig. S9). The interaction between RNPS1 and MAGOH (EJC complex) was also diminished by the RNPS1^{F181I} mutation (Fig. 5*A*), which was supported by a $\Delta G_{F181I\text{-}WT}$ of 31.2 kcal/mol for the complex of RNPS1+EIF4A3+MAGOH+UPF3B (21) (*SI Appendix*, Table S1). We also observed similar subcellular localization of RNPS1^{WT} and RNPS1^{F181I} in HEK293T cells. We hypothesized that the reduced interaction of RNPS1^{F181I} with complex constituents may impair the formation and/or function of the EJC, PSAP, and/or ASAP complexes, resulting in splicing alterations and subsequent transcript and protein expression changes. We therefore undertook analyses of the transcriptome, proteome, and splicing in *Rnps1*$^{F181I/F181I}$ and WT CD8$^+$ T cells and HSCs.

By RNA sequencing (RNA-seq) analysis, we identified 267 transcripts that were differentially expressed between *Rnps1*$^{F181I/F181I}$ and WT splenic CD8$^+$ T cells, with 90 up-regulated and 177 down-regulated transcripts in *Rnps1*$^{F181I/F181I}$ cells (Dataset S1). We used the DAVID Functional Annotation Tool to identify highly represented Gene Ontology (GO) terms and Kyoto Encyclopedia of Genes and Genomes (KEGG) pathways among transcripts with differential expression. However, no GO terms or signaling pathways were enriched among up-regulated transcripts (Dataset S1). Enrichment of genes (false discovery rate [FDR] < 0.05) associated with KEGG pathways "*Staphylococcus aureus* infection," "protein digestion and absorption," and "fat digestion and absorption" and with GO term "antigen processing and presentation of exogenous peptide antigen via major histocompatibility complex (MHC) class II" was found among transcripts down-regulated in *Rnps1*$^{F181I/F181I}$ CD8$^+$ T cells (Dataset S1).

We analyzed NMD and splicing in the RNA-seq data from splenic CD8$^+$ T cells and HSCs isolated from *Rnps1*$^{F181I/F181I}$ versus *Rnps1*$^{+/+}$ littermates. Analysis of premature stop codons suggested that NMD was not impaired in *Rnps1*$^{F181I/F181I}$ cells (*SI Appendix*, Fig. S10 *A* and *B* and Supplementary Text). A total of 1,113 splicing variations were detected at significantly different frequencies in untreated *Rnps1*$^{F181I/F181I}$ versus *Rnps1*$^{+/+}$ splenic CD8$^+$ T cells (Fig. 5 *B* and *C* and Dataset S4); all analyzed variants were present in both *Rnps1*$^{F181I/F181I}$ and *Rnps1*$^{+/+}$ cells. Three types of variation were detected: intron retention (IR; 795 transcripts), exon skipping (ES; 274 transcripts), and cryptic splice (CS) site usage (44 transcripts). We found that the majority of IR events (750/795; 94.3%) and ES events (198/274; 72%) occurred more frequently in *Rnps1*$^{F181I/F181I}$ splenic CD8$^+$ T cells than in WT cells, while the majority of CS events were more frequent (38/44; 86.4%) in *Rnps1*$^{+/+}$ splenic CD8$^+$ T cells (Fig. 5 *B* and *C* and Dataset S4). We verified selected splice variants by RT-PCR using RNA from *Rnps1*$^{F181I/F181I}$ and *Rnps1*$^{+/+}$ splenic CD8$^+$ T cells (*SI Appendix*, Fig. S10*I* and Supplementary Text and Dataset S10).

In HSCs, 396 splicing variations were detected at significantly different frequencies in *Rnps1*$^{F181I/F181I}$ versus *Rnps1*$^{+/+}$ HSCs (*SI Appendix*, Fig. S10 *C* and *D* and Dataset S5). Similar to CD8$^+$ T cells, the majority of IR events (228/296; 77%) and ES events (63/80; 78.8%) occurred more frequently in *Rnps1*$^{F181I/F181I}$ HSCs than in WT cells; in contrast, the majority of CS events were more frequent (17/20; 85%) in *Rnps1*$^{+/+}$ HSCs than in *Rnps1*$^{F181I/F181I}$ cells (*SI Appendix*, Fig. S10 *C* and *D* and Dataset S5). These data strongly suggest that

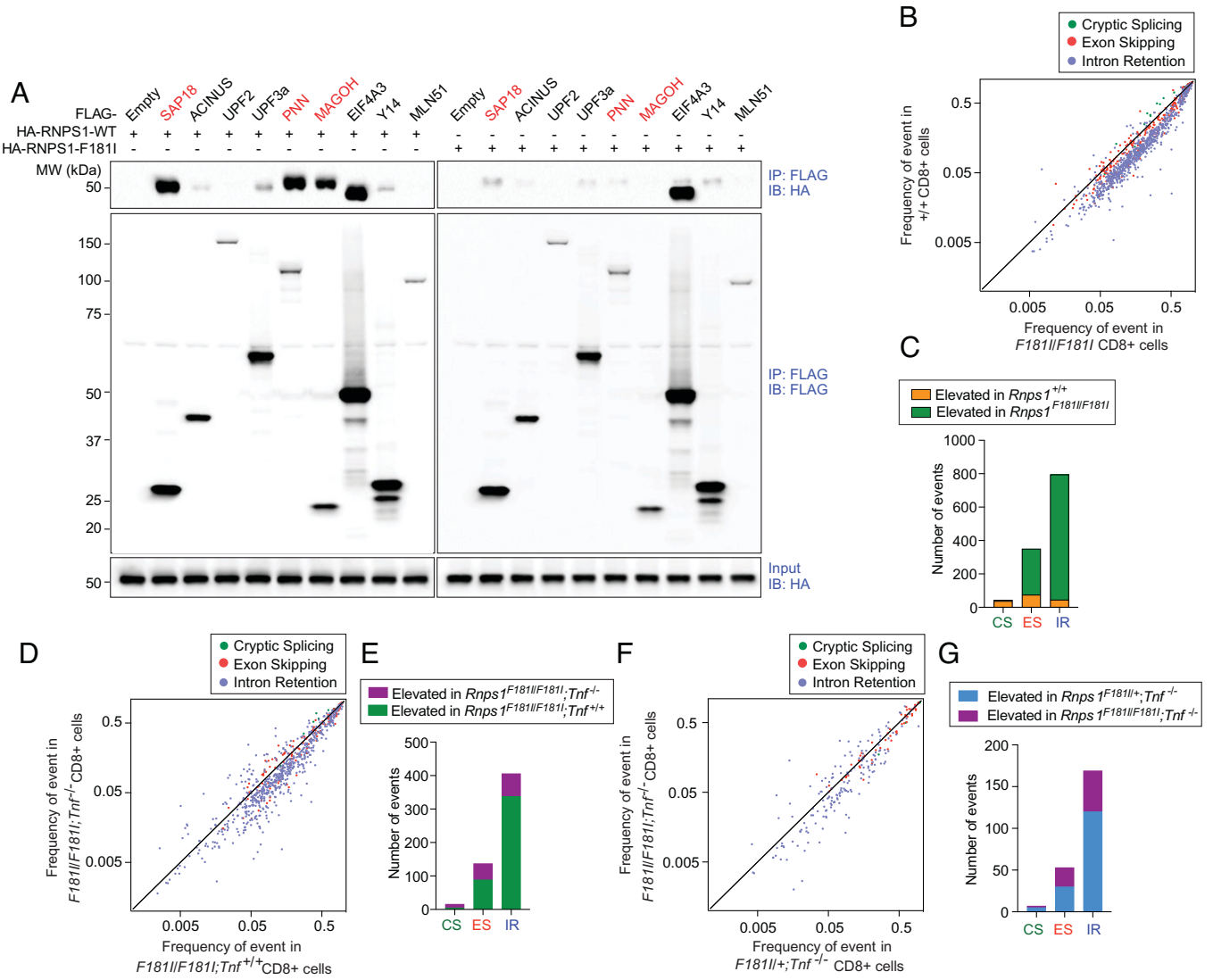

Fig. 5. Magnified IR and ES in primary *F181I/F181I* CD8$^+$ T cells. (*A*) HEK293T cells were transfected with FLAG-tagged SAP18, ACINUS, UPF2, UPF3a, PNN, MAGOH, EIF4A3, Y14, MLN51, or empty vector and HA-tagged WT RNPS1 or RNPS1^{F181I}. Lysates were subsequently immunoprecipitated by using anti-FLAG M2 agarose and immunoblotted with antibodies against HA or FLAG. Experiments were performed three times. (*B*, *D*, and *F*) Comparative analysis of the frequency of splicing variations in *Rnps1*$^{F181I/F181I}$ versus *Rnps1*$^{+/+}$ splenic CD8$^+$ T cells (*B*), *Rnps1*$^{F181I/F181I}$ versus *Rnps1*$^{F181I/F181I}$;*Tnf*$^{-/-}$ splenic CD8$^+$ T cells (*D*), and *Rnps1*$^{F181I/+}$;*Tnf*$^{-/-}$ versus *Rnps1*$^{F181I/F181I}$;*Tnf*$^{-/-}$ splenic CD8$^+$ T cells (*F*). Each symbol represents one splicing variant in a particular transcript. The frequency of the variant among total sequences containing that junction is plotted (PIR/PSI for CS and IR; 1-PSI for ES). The diagonal line represents equal frequency in the two groups. Only splice variants detected at different frequencies between groups are plotted. (*C*, *E*, and *G*) Quantitative analysis of splicing events in *Rnps1*$^{F181I/F181I}$ versus *Rnps1*$^{+/+}$ splenic CD8$^+$ T cells (*C*), *Rnps1*$^{F181I/F181I}$ versus *Rnps1*$^{F181I/F181I}$;*Tnf*$^{-/-}$ splenic CD8$^+$ T cells (*E*), and *Rnps1*$^{F181I/+}$;*Tnf*$^{-/-}$ versus *Rnps1*$^{F181I/F181I}$;*Tnf*$^{-/-}$ splenic CD8$^+$ T cells (*G*). The experiment was performed one time (n = 2 or 3 mice/genotype). $^{+/+}$ indicates WT, and *F181I/F181I* indicates the *Rnps1*$^{F181I/F181I}$ genotype. MW, molecular weight; IP, immunoprecipitation; IB, immunoblot.

RNPS1^{F181I} supports reduced splicing activity compared to RNPS1^{WT}.

We also conducted splicing analysis for *Rnps1*$^{F181I/F181I}$;*Tnf*$^{-/-}$ splenic CD8$^+$ T cells and HSCs, comparing their frequencies of splicing variations with those in *Rnps1*$^{F181I/F181I}$;*Tnf*$^{+/+}$ cells and with those in *Rnps1*$^{F181I/+}$;*Tnf*$^{-/-}$ cells; 559 variations were detected at significantly different frequencies in *Rnps1*$^{F181I/F181I}$;*Tnf*$^{-/-}$ versus *Rnps1*$^{F181I/F181I}$;*Tnf*$^{+/+}$ splenic CD8$^+$ T cells (Fig. 5 *D* and *E* and Dataset S6). Notably, 153 of the 559 splicing variations were also detected in *Rnps1*$^{F181I/F181I}$ versus *Rnps1*$^{+/+}$ CD8$^+$ T cells; these shared variations are apparently dependent on TNF expression by *Rnps1*$^{F181I/F181I}$ cells. The majority of IR events (337/406; 83%) and ES events (89/137; 65%) occurred more frequently in *Rnps1*$^{F181I/F181I}$;*Tnf*$^{+/+}$ splenic CD8$^+$ T cells than in *Rnps1*$^{F181I/F181I}$;*Tnf*$^{-/-}$ cells (Fig. 5 *D* and *E* and Dataset S6). Similarly, 402 variations were detected at significantly different frequencies in *Rnps1*$^{F181I/F181I}$;*Tnf*$^{-/-}$ versus *Rnps1*$^{F181I/F181I}$;*Tnf*$^{+/+}$ HSCs, and the majority of IR events (238/343; 69%) occurred more frequently in *Rnps1*$^{F181I/F181I}$;*Tnf*$^{+/+}$ HSCs than in *Rnps1*$^{F181I/F181I}$;*Tnf*$^{-/-}$ cells (*SI Appendix*, Fig. S10 *E* and *F* and Dataset S7). These data indicate that knockout of TNF reduces the frequency of IR and ES events caused by homozygosity for *Rnps1*^{F181I} and strongly suggest that a portion of splicing variations with different frequencies in *Rnps1*$^{F181I/F181I}$ versus *Rnps1*$^{+/+}$ are secondary to the elevated TNF produced in *Rnps1*$^{F181I/F181I}$ mice.

Consistent with this idea, analysis of splicing variations between *Rnps1*$^{F181I/F181I}$;*Tnf*$^{-/-}$ and *Rnps1*$^{F181I/+}$;*Tnf*$^{-/-}$ cells revealed only 229 variations for CD8$^+$ T cells (Fig. 5 *F* and *G* and Dataset S8) and 301 variations for HSCs (*SI Appendix*, Fig. S10 *G* and *H* and Dataset S9). This represents a reduction

of 79.4% from the number of splicing variations with different frequencies between *Rnps1*$^{F181I/F181I}$ and *Rnps1*$^{+/+}$ CD8$^+$ T cells and a 24.0% reduction from that number for HSCs. Moreover, in the *Tnf*$^{-/-}$ background, frequencies of IR and ES events are no longer skewed toward the *Rnps1*$^{F181I/F181I}$ genotype, but toward the *Rnps1*$^{F181I/+}$ genotype (Fig. 5 *F* and *G*, and *SI Appendix*, Fig. S10 *G* and *H*). These findings indicate that TNF knockout eliminates many of the splicing variation differences between *Rnps1*$^{F181I/F181I}$ cells and RNPS1-sufficient cells, particularly the differences in frequencies of IR events. These findings support the hypothesis that elevated TNF may contribute significantly to splicing alterations in *Rnps1*$^{F181I/F181}$ cells.

Discussion

We identified a viable hypomorphic allele of mouse *Rnps1*, permitting an in-depth analysis of the physiological effects of RNPS1 loss of function in the hematopoietic system. *Rnps1*$^{F181I/F181I}$ mice displayed reduced numbers of hematopoietic stem and progenitor cells and pancytopenia in the blood. These deficits were restricted to *Rnps1*$^{F181I/F181I}$ cells in mixed bone marrow chimeras, indicating they were hematopoietic cell intrinsic. We have investigated the mechanisms by which RNPS1 loss of function causes HSC and T cell deficiencies, and our findings highlight the role of chronic, excessive TNF in these phenotypes.

TNF has been observed to have both stimulatory and suppressive effects on HSC self-renewal and maintenance (22–26). In 2019, a report by Yamashita and Passegué (23) helped to explain these discrepancies by examining the effects on specific HSC and progenitor subpopulations of direct injection of TNF into mice. They showed that TNF induced myeloid progenitor apoptosis while promoting HSC survival and myeloid differentiation through activation of a strong and specific NF-κB (p65)–dependent gene program (23). Importantly, the effect of TNF in sustaining HSCs and promoting myeloid differentiation was eliminated when TNF was supplied chronically rather than transiently; with chronic TNF stimulation, the produced myeloid cells were killed by apoptosis (23). Our data revealed that deletion of TNF in *Rnps1*$^{F181I/F181I}$ mice rescued all of the HSC and progenitor populations and most of the blood cell populations to normal or near-normal numbers. The findings of Yamashita and Passegué (23) are consistent with our own and support the conclusion that constitutive, excessive TNF contributes to the death of HSCs and progenitor cells in *Rnps1*$^{F181I/F181I}$ mice. In further support of this idea, we detected an average of ∼10 pg/mL of soluble TNF in the serum of 12- to 14-wk-old *Rnps1*$^{F181I/F181I}$ mice, with concentrations reaching ∼30 pg/mL in some animals, while TNF was maintained at nearly undetectable levels in the serum of WT mice. We have not measured TNF concentration in the bone marrow, where it is typically undetectable (23), but suspect that its local concentration may be higher there, considering that *Rnps1*$^{F181I/F181I}$ hematopoietic cells are a significant source of TNF.

By examining caspase activation in CD8$^+$ T cells, we discovered that TNF-stimulated apoptosis of *Rnps1*$^{F181I/F181I}$ CD8$^+$ T cells was caused by hyperactivity of the extrinsic apoptotic pathway. Moreover, *Rnps1*$^{F181I/F181I}$ CD8$^+$ T cells expressed elevated amounts of TNF-R2 protein, suggesting that they may be hypersensitive to TNF stimulation. Previous publications have shown that the ASAP complex promotes apoptosis, after which it is disassembled (5, 6). However, we found that RNPS1^{F181I} binds poorly to SAP18 compared with RNPS1^{WT}, suggesting that ASAP complex functions may be compromised in *Rnps1*$^{F181I/F181I}$ cells. We observed a slightly elevated level of BCL-XS in *Rnps1*$^{F181I/F181I}$ CD8$^+$ T cells after TNF stimulation, consistent with a report that knockdown of RNPS1 increased the transcript level of BCL-XS by more than 10% in HeLa and HEK293T cells lines and promoted apoptosis (7). It was also reported that knockdown of RNPS1 promoted alternative splicing to produce proapoptotic splice variants of numerous transcripts, including *Mcl1* and Bcl-2 family proteins *Bcl-x* and *Bim*, which encode mediators of the intrinsic apoptotic pathway (7, 27–29); this effect was not mediated by the EJC function of RNPS1, but through RNPS1 interaction with a *cis* regulatory sequence distant from the splice site. Our findings support previous data showing that RNPS1 is an important regulator of apoptosis, but we demonstrated that cell death caused by RNPS1 deficiency is induced in a TNF-dependent manner that activates the extrinsic apoptotic pathway, at least in CD8$^+$ T cells. The death of HSCs was also TNF dependent.

The F181I mutation of RNPS1 caused changes in splicing and transcript expression across the genome. Based upon our examination of the effects of RNPS1^{F181I} on splicing, we conclude that WT RNPS1 promotes proper splicing in that RNPS1 deficiency in HSCs or CD8$^+$ T cells led to elevated frequencies of hundreds of IR and ES events compared to those in WT cells. Interestingly, the elevated frequencies of most IR and ES events in *Rnps1*$^{F181I/F181I}$ CD8$^+$ T cells were reduced to normal levels by knockout of TNF. We speculate that TNF signaling induces a transcriptional program requiring the simultaneous up-regulation of splicing in *Rnps1*$^{F181I/F181I}$ cells. However, errors in these splicing events accumulated in *Rnps1*$^{F181I/F181I}$ cells and were detected as increased IR and ES events. In the absence of TNF, the TNF-induced transcriptional program is not activated, and IR and ES events are reduced. Splicing analysis also indicated numerous differences in frequencies of IR and ES events between WT CD8$^+$ T cells and *Rnps1*$^{F181I/F181I}$;*Tnf*$^{-/-}$ cells, suggesting that TNF knockout does not return *Rnps1*$^{F181I/F181I}$ cells to a WT state.

We do not understand the trigger for TNF production in *Rnps1*$^{F181I/F181I}$ cells. No alterations of splicing were detected in *Tnf* transcripts nor in *Tnfr2*, *Tnfrsf8*, *Tnfaip3* (encoding A20), or *Nfkbia* (encoding IκBα) transcripts in *Rnps1*$^{F181I/F181I}$ cells. We conclude that excessive TNF production and TNF pathway protein expression observed in *Rnps1*$^{F181I/F181I}$ mice are not due to failure in the splicing of *Tnf* itself or transcripts encoding TNF signaling pathway proteins. We could identify putative TNF-independent splicing defects by comparing the splicing analysis of *Rnps1*$^{+/+}$ versus *Rnps1*$^{F181I/F181I}$ cells with the analysis of *Rnps1*$^{F181I/F181I}$;*Tnf*$^{-/-}$ versus *Rnps1*$^{F181I/+}$;*Tnf*$^{-/-}$ cells. Transcripts affected in both analyses were candidates whose aberrant splicing might underlie the up-regulation of TNF in *Rnps1*$^{F181I/F181I}$ cells. However, among the 83 candidates identified in this way, the transcript expression level of only one was also altered (*Plbd1*, down-regulated in *Rnps1*$^{F181I/F181I}$ cells). It remains possible that an indirect effect of global changes in splicing, transcript, and protein expression caused by RNPS1 deficiency during the normal course of hematopoietic development and expansion results in elevated TNF production.

Another intriguing possibility relates to a reported role for RNPS1 in suppressing R-loops (30), RNA-DNA hybrids generated, for example, during transcription. R-loops have been shown to activate cyclic GMP-AMP synthase (cGAS)-stimulator of interferon genes (STING)–mediated inflammatory signaling (31, 32). Interestingly, although *Rnps1*$^{F181I/F181I}$ macrophages showed normal TNF production in response to ligands for TLR4, TLR2/1, TLR3, TLR7, and TLR9, elevated IFN-α production in response to cytosolic dsDNA, a cGAS ligand, was observed in

Rnps1$^{F181I/F181I}$ macrophages. Therefore, a failure of RNPS1 to suppress or resolve R-loops may result in constitutive inflammatory signaling and excessive TNF production.

The hematopoietic phenotype of *Rnps1*$^{F181I/F181I}$ mice bears some resemblance to myelodysplastic syndrome (MDS), in which dysplastic HSCs fail to develop into mature blood cells. Necessary diagnostic criteria for MDS in mice are cytopenia in at least one lineage (anemia, neutropenia, and thrombocytopenia all present in *Rnps1*$^{F181I/F181I}$ mice) and cytologic or histologic evidence of dysplasia with or without increased numbers of immature nonlymphoid cells (33) (not examined in *Rnps1*$^{F181I/F181I}$ mice). Molecular evidence of a monoclonal cell population is supportive of MDS (33). Mutations in multiple general splicing factors (*SF3B1*, *SRSF2*, *U2AF1*, *U2AF2*, and *ZRSR2*) have been linked to MDS (34), and an increase in R-loops has been proposed as a unifying mechanism for causation of MDS despite distinct patterns of splicing defects (35, 36). Additionally, elevated levels of TNF have been detected in bone marrow biopsies, plasma, and serum and in cultured cells from MDS patients, particularly those with low-risk MDS (37–41). Future studies should formally exclude or diagnose MDS in *Rnps1*$^{F181I/F181I}$ mice. If present in mice, our findings suggest that *RNPS1* mutations may be a previously unappreciated cause of MDS in humans. Overall, our findings illuminate a link between RNPS1-dependent splicing regulation and TNF, in which RNPS1 is necessary to limit TNF-dependent cell death and support hematopoiesis.

Materials and Methods

Sources of mice are provided in *SI Appendix, Supplementary Materials and Methods*.

Flow Cytometry. Peripheral blood was collected from G3 mice >6 wk old by cheek bleeding. The red blood cell (RBC)-depleted samples were stained for 1 h at 4 °C in 100 μL of a 1:200 mixture of fluorescence-conjugated antibodies to 15 cell surface markers encompassing the major immune lineages (*SI Appendix, Supplementary Materials and Methods*). Flow cytometry data were collected on a BD LSR Fortessa, and the proportions of immune cell populations in each G3 mouse were analyzed with FlowJo software. The resulting screening data were uploaded to Mutagenetix for automated mapping of causative alleles. Procedures and antibodies for staining B cells, T cells, HSCs, hematopoietic progenitors, and intracytoplasmic cytokines are provided in *SI Appendix, Supplementary Materials and Methods*.

HSC Sorting and Bone Marrow Chimeras. For HSC sorting, $^{+/+}$ (CD45.2), *F181I/F181I* (CD45.2), or $^{+/+}$ (CD45.1) bone marrows were stained with Alexa Fluor 700 anti-mouse lineage mixture: B220, CD3, CD11b, Ly-6G/6C, and Ter-119 antibodies (Biolegend, clones 17A2/RB6-8C5/RA3-6B2/Ter-119/M1/70), Ly-6A/E (Sca-1) (Biolegend, clone D7), and CD117 (c-kit) (Biolegend, clone 2B8) and then sorted using the fluorescence-activated cell sorter (FACS) Aria II SORP or FACS Aria Fusion cell sorter (BD Biosciences).

Recipient mice were lethally irradiated with two 7-Gy exposures to X-irradiation administered 5 h apart. Femurs derived from donor C57BL/6.SJL (CD45.1) or CRISPR-F181I (CD45.2) homozygotes were flushed with phosphate-buffered saline (PBS) using a 25G needle. To remove bits of bone, the marrow was homogenized, and the solution was passed through a sterile 40-μm nylon cell strainer (BD Biosciences). The volume was brought to 50 mL with medium and then centrifuged at 700 × *g* for 5 min at 4 °C. The cells were then resuspended in 5 mL of RBC lysis buffer (Sigma-Aldrich) and incubated for 1 to 2 min. The cells were centrifuged at 700 × *g* for 5 min, and cells were resuspended in 1 mL PBS and transferred into 1.5-mL Eppendorf tubes and kept on ice. A 1:1 mixture of bone marrow cells or purified HSCs from C57BL/6.SJL mice (CD45.1) and CRISPR-F181I mice (CD45.2) or WT littermates (CD45.2) was transferred into the indicated recipient mice through retro-orbital injection. For 4 wk after engraftment, mice were maintained on antibiotics. Twelve weeks after bone marrow transplantation, peripheral blood was sampled and assessed with flow cytometry using fluorescence-conjugated antibodies against the CD45 congenic markers [CD45.1 (Biolegend, cloneA10), CD45.2 (Biolegend, clone 104)].

Detection of Apoptosis. Annexin V labeling and detection were performed with the fluorescein isothiocyanate–annexin V apoptosis detection Kit I (BD Biosciences) following the manufacturer's instructions.

Immunization and Enzyme-Linked Immunosorbent Assay Analysis. Twelve- to sixteen-week-old mice were intramuscularly immunized with OVA (200 μg; Invivogen) with alum (20 μg, Invivogen) as adjuvant on day 0 and intraperitoneally immunized with NP_{50}-AECM-Ficoll (50 μg, Biosearch Technologies) on day 8 as previously described (42). Blood was collected on day 6 after NP-Ficoll immunization in minicollect tubes (Mercedes Medical) and centrifuged at 1,500 × *g* to separate serum for determination of antigen-specific immunoglobulin (Ig)G or IgM concentration by enzyme-linked immunosorbent assay (ELISA) using standard methods (*SI Appendix, Supplementary Materials and Methods*).

To detect TNF production, blood from 12- to 14-wk-old *Rnps1*$^{+/+}$;*Tnf* $^{-/-}$, *Rnps1*$^{+/+}$;*Tnf* $^{+/+}$, *Rnps1*$^{F181I/F181I}$;*Tnf* $^{+/+}$, and *Rnps1*$^{F181I/F181I}$;*Tnf* $^{-/-}$ mice was collected and centrifuged at 1,500 × *g* to separate serum. WT or *Rnps1*-KO EL4 cells (2 x 10^4/well) were plated in 96-well plates. Cell media were collected 72 h after plating. Mouse serum or cell media were assayed using TNF mouse uncoated ELISA kit (Thermo Fisher Scientific) or IFN-α mouse precoated ELISA kit (Thermo Fisher Scientific) according to the manufacturer's instructions.

B-cell activating factor (BAFF) concentrations in serum from 6- to 8-wk-old *Rnps1*$^{F181I/F181I}$ and WT littermates were analyzed by BAFF ELISA Kit (Thermo Fisher Scientific).

In Vivo NK Cell and CD8$^+$ T Cell Cytotoxicity Analyses. Cytolytic CD8$^+$ T cell effector function and NK cell–mediated killing were measured by standard in vivo CTL assay or NK cell killing assay (*SI Appendix, Supplementary Materials and Methods*).

MCMV Challenge and Quantification. MCMV (Smith strain) was administered by intraperitoneal injection at 10^5 plaque-forming units (PFUs) per 20 g body weight as described previously (43). Five days later, ~30 mg of spleen was harvested from each mouse. Total genomic DNA (including from mouse host and MCMV virus) was extracted by incubating the tissues in 200 μL of 1X PCR Buffer with Nonionic Detergents (PBND) buffer [10 mM Tris·HCl, pH 8.3, 50 mM KCl, 2.5 mM $MgCl_2$, 0.1 mg/mL gelatin, 0.45% (vol/vol) IGEPAL CA-630, and 0.45% (vol/vol) Tween 20] supplemented with 100 μg/mL proteinase K at 56 °C overnight. Then, the supernatant DNA was incubated at 95 °C for 15 min to inactivate the proteinase K and then diluted 100× and directly used for quantification of the copy number of both mouse genome (represented by mouse gene *Actb*) and MCMV genome (represented by MCMV immediate-early gene *IE1*) by real-time qPCR. The viral titer was expressed as the copy number ratio of MCMV genome versus mouse genome (shown in $\log_{10}$). The real-time qPCR primers are listed in *SI Appendix*, Table S2.

In Vivo T Cell Proliferation. To detect antigen-specific T cell expansion, splenic OT-I or OT-II T cells were isolated from *Rnps1*$^{F181I/F181I}$ or WT littermates using the EasySep mouse CD8$^+$ (or CD4$^+$) T cell isolation kit (StemCell Technologies) and stained for 20 min at 37 °C with 5 μM CellTrace Violet dye (*Rnps1*$^{F181I/F181I}$ T cells) (Life Technologies) or CellTrace Far Red dye (WT T cells) (Life Technologies). A 1:1 mix of labeled *Rnps1*$^{F181I/F181I}$ and WT cells was intravitreally injected to CD45.1 mice. The next day, 100 μg of OVA in 200 μL of PBS or 200 μL of sterile PBS as a control was intraperitoneally injected into the recipients. The marked cells were analyzed at 48 h after immunization, using a FACS LSR (Becton Dickinson). To assess the homeostatic T cell proliferation, splenic pan-T cells from CD45.1 (WT) or CD45.2 (*Rnps1*$^{F181I/F181I}$) mice were isolated by using the EasySep mouse pan-T cell isolation kit (StemCell Technologies). Pan-T cells were labeled for 20 min at 37 °C with 5 μM CellTrace Far Red dye (Life Technologies) and were intravenously injected into irradiated recipients with a 1:1 mix of CD45.1 and CD45.2 cells. The marked cells were analyzed at day 7 after injection using annexin V, CD4 (BD Biosciences, clone RM4-5), and CD8α (Biolegend, clone 53-6.7) staining by a FACS LSR (Becton Dickinson).

Measurement of Cytokine Production by Peritoneal Macrophages. Four days after intraperitoneal injection of 2 mL of BBL thioglycollate medium [4% (wt/vol) brewer's thioglycollate medium power (BD Biosciences)], thioglycollate-elicited macrophages were recovered in 5 mL of PBS by peritoneal lavage. Cells were seeded onto 96-well plates at 1×10^5 cells per well and cultured in Dulbecco's modified Eagle's medium (DMEM) containing 10% fetal bovine serum (FBS) (Gibco), 1% penicillin/streptomycin (Life Technologies) at 37 °C, and 5% CO_2. Macrophages were stimulated for 4 h with Pam3CSK4 (40 ng/mL), poly(I:C) (20 μg/mL), lipopolysaccharide (LPS) (10 ng/mL), R848 (25 ng/mL) (all from Enzo Life Science), or CpG (Sigma-Aldrich, 100 μg/mL). dsDNA (IDT, 2 μg/mL) was complexed with Lipofectamine 2000 (Life Technologies) and transfected according to the manufacturer's instructions. Nigericin (Sigma-Aldrich, 10 μg/mL) stimulation for 1 h was performed after 4-h LPS priming (10 ng/mL). Cytokine concentrations in the supernatants were measured using ELISA kits for mouse IFN-α, interleukin-1β, and TNF (eBioscience).

Generation of *Rnps1* Knockout EL4 Cells Using the CRISPR-Cas9 System. To generate *Rnps1*-KO EL4 cell lines, mouse EL4 cells (T cell line) were transfected with a *PX458* plasmid encoding a small base-pairing guide RNA targeting the genomic locus of mouse *Rnps1* (5′-caggaagctccagcacgtcc-3′) and green fluorescent protein (GFP). Forty-eight hours after transfection, GFP^+ cells were sorted by flow cytometry, and single colonies were selected by a limiting dilution assay. The single colonies were screened and confirmed by immunoblotting using an RNPS1 antibody (GeneTex, GTX129789).

Plasmids. WT or F181I mouse RNPS1 (NM_009070) was tagged with an N-terminal HA epitope in pCMV6 vector. Amino acids 255 to 581 of mouse ACINUS (NM_019567) and full-length mouse SAP18 (NM_009119), UPF2 (NM_001081132), UPF3A (NM_025924), PNN (NM_008891), MAGOH (NM_001282737), EIF4A3 (NM_138669), Y14 (NM_001039518), and MLN51 (NM_138660) were cloned into pCDNA6 vector with a FLAG epitope. Plasmids were sequenced to confirm the absence of undesirable mutations.

In Vitro Stimulation of T Cells. Splenic $CD8^+$ T cells were negatively enriched using the EasySep Mouse $CD8^+$ T Cell Isolation Kit (StemCell Technologies). For the in vitro stimulation assay, 3×10^6 $CD8^+$ T cells were treated for 4 h at 37 °C with either vehicle (sterile PBS), recombinant mouse TNF (50 ng/mL) (ENZO Life Sciences), or FasL (25 ng/mL) (R&D Systems). *Rnps1*$^{+/+}$ or *Rnps1*-KO EL4 T cells (1×10^6/well) were treated with vehicle (sterile PBS), recombinant mouse TNF (50 ng/mL) for 4 h, or 100 ng/mL mouse TNF neutralizing rabbit antibody (CST, clone D2H4) for 72 h. Then, the cells were washed twice in sterile PBS to remove residual proteins in the culture media. Proteins levels were measured using immunoblot.

Cell Culture, Transfection, Co-IP, and Immunoblotting. HEK293T cells were grown at 37 °C in DMEM (Life Technologies) supplemented with 10% (vol/vol) FBS (Gibco) and 1% penicillin-streptomycin (Life Technologies) in 5% CO_2. Transfection of plasmids was carried out using Lipofectamine 2000 (Life Technologies) according to the manufacturer's instructions. Thirty-six to 48 h after transfection, cells were harvested in Nonidet P-40 lysis buffer [20 mM Tris–Cl, pH 7.5, 150 mM NaCl, 1 mM ethylenediaminetetraacetic acid, 1 mM ethylene glycol tetraacetic acid (EGTA) , 1% (vol/vol) Nonidet P-40, 2.5 mM $Na_4P_2O_7$, 1 mM $C_3H_9O_6P$, 1 mM Na_3VO_4, and protease inhibitors] for 45 min at 4 °C. Co-IP assays were performed using cell extracts from HEK293T cells overexpressing WT RNPS1, $RNPS1^{F181I}$, truncated mouse ACINUS, full-length mouse SAP18, UPF2, UPF3A, PNN, MAGOH, EIF4A3, Y14, and MLN51 proteins. Cell extracts were mixed, and proteins were immunoprecipitated by anti-FLAG M2 affinity gel (Sigma-Aldrich). Captured proteins were eluted in PBS with 30 μL of 200 μg/mL 3×FLAG peptides (Sigma-Aldrich) and 8 μL of sample buffer mixed with 0.1% bromophenol blue, heated to 95 °C for 3 min. Samples were centrifuged at $12{,}000 \times g$ for 1 min, and then the supernatants were subjected to sodium dodecyl sulfate (SDS)–polyacrylamide gel electrophoresis for immunoblotting analysis by anti-FLAG (Sigma-Aldrich, clone M2) and anti-HA (CST, clone C19F4), as described below.

For direct immunoblot analysis of $CD8^+$ T cells, splenic $CD8^+$ T cells were enriched using EasySep Mouse $CD8^+$ T Cell Isolation Kit (StemCell Technologies). Approximately 10^6 unstimulated or stimulated $CD8^+$ or EL4 T cells were lysed in buffer [1% SDS (Thermo Fisher Scientific), 1:10,000 Benzonase (Sigma-Aldrich), and 1:100 Protease Inhibitor Mixture (Cell Signaling Technology) in buffer A (50 mM 4-(2-hydroxyethyl)-1-piperazineethanesulfonic acid (Hepes), 2 mM $MgCl_2$, and 10 mM KCl)] and analyzed by standard immunoblot analysis using the antibodies listed in *SI Appendix, Supplementary Materials and Methods*.

rmsd MD Simulation Analysis. Three systems (ASAP, PSAP, and EJC complex) were used for rmsd analysis to predict the $RNPS^{1F181I}$ interaction changes. For system 1, three domains, RNPS1 (Residue IDs 1 to 88), SAP18 (120 to 244), and Acinus (89 to 115), were included in the rmsd analysis. For system 2, three domains, RNPS1 (Residue IDs 1 to 88), SAP18 (120 to 244), and PNN (89 to 119), were included in the rmsd analysis. For system 3, four domains, RNPS1 (Residue IDs 534 to 621), MAGOH (391 to 533), EIF4A3 (1 to 390), and UPF3B (622 to 636), were included in the rmsd analysis. The F181I substitution was included (renumbered as F25I in systems 1 and 2, as F558I in system 3). After the stepwise minimizations, the MD equilibrium phase, 2,500 MD snapshots were evenly selected from 1-ms MD trajectories for post-MD analysis. We calculated average structures for both $RNPS1^{WT}$ and $RNPS1^{F181I}$. Then, we calculated the residue–residue correlations following a computation protocol proposed by Kong and Karplus (44). We improved their protocol by including the solvation free energies in residue–residue correlation calculation. The MD system setup and MD simulation protocol were described previously (45–48).

Standard Growth Curve. Live *Rnps1*$^{+/+}$ or *Rnps1*-KO EL4 cells (1×10^4/well) were treated with 100 ng/mL mouse TNF neutralizing rabbit antibody (CST, clone D2H4) or isotype control for 7 d. Every 24 h, the cells were centrifuged at $700 \times g$ for 5 min and resuspended in 20 μl PBS. Suspended cells (10 μL) and an equal volume of Trypan Blue (10 μL) were mixed to count the total number of cells using a TC20 Automated Cell Counter (Bio-Rad). A standard growth curve was generated by graphing cell counts every 24 h.

PTC and Splicing Variation Analysis. Splenic $CD8^+$ T cells or HSCs from individual *Rnps1*$^{+/+}$;*Tnf* $^{+/+}$, *Rnps1*$^{+/+}$;*Tnf* $^{--}$, *Rnps1*$^{F181I/F181I}$;*Tnf* $^{+/+}$, or *Rnps1*$^{F181I/F181I}$;*Tnf* $^{-/-}$ mice were negatively enriched using the EasySep Mouse $CD8^+$ T Cell or HSC Isolation Kit (StemCell Technologies). Total RNAs from these cells were extracted using the RNeasy Plus kit with genomic DNA elimination (Qiagen). Libraries were generated using the KAPA Stranded RNA-Seq Kit with RiboErase (HMR) (Kapa Biosystems). Paired-end 2 × 100–bp sequencing was performed using an Illumina HiSEq. 2500. For RNA-seq data analysis, reads were de-multiplexed using CASAVA, and tophat (v.2.0.10) was used to map the reads to the mouse transcriptome (build mm10). Cufflinks and cuffmerge (v.2.1.1) were then used to calculate fragments per kilobase of transcript per million reads mapped and consolidate results across the samples (data were averaged for each genotype/treatment combination). Finally, cuffdiff (v.2.1.1) was used to calculate log-fold changes and the associated statistics. The R package of IsoformSwitchAnalyzeR was used to analyze PTC-containing transcript accumulations. *Q* values were FDR-corrected *P* values calculated by IsoformSwitchAnalyzeR. Isoform frequency expressed as *F181I/F181I:* $^{+/+}$ ($\log_2$) versus switch *Q* value (−log10) was plotted in the graph.

For splicing analysis, reads from mapped bam files for each sample were separated by chromosome due to size. The chromosomal bam files were then fed to ASpli (49, 50), using the GRCm38 reference gene transfer file for gene annotation and read quantification. Based on reference genome annotations for exons and introns, counts of reads spanning junctions between exons as well as those that read from exon into intron were gathered. These counts were then analyzed via the AsDiscover function of ASpli to annotate junctions, and Percent Intron Retention (PIR) or Percent Sequence Inclusion (PSI) metrics were output for all alternate splicing events as described (https://bioconductor.org/packages/release/bioc/vignettes/ASpli/inst/doc/ASpli.pdf). Once junctions were collected and analyzed for alternate splicing, the junctionDUReport function was used to generate lists of differentially expressed junctions, with their associated *P* values. Splicing events for which any junction returned a read value of not available ("NA") were eliminated from further analysis and from the datasets.

RNA Preparation, Reverse Transcription, and RT-PCR. RNA from total splenic $CD8^+$ T cells from *Rnps1*$^{+/+}$;*Tnf* $^{+/+}$, *Rnps1*$^{+/+}$;*Tnf* $^{-/-}$, *Rnps1*$^{F181I/F181I}$;*Tnf* $^{+/+}$, or *Rnps1*$^{F181I/F181I}$;*Tnf* $^{-/-}$ mice was extracted using TRIzol reagent (Sigma-Aldrich) and treated with RQ1 ribonuclease-free deoxyribonuclease

(DNase I) (Promega) at 37 °C for 30 min to remove contaminating genomic DNA. DNase I was heat inactivated by heating to 65 °C for 10 min. Equal amounts (1 μg) of RNA were used for reverse transcription using an oligo (dT) primer (Promega) and ImProm-II reverse transcriptase (Promega) following the manufacturer's instructions. RT-PCR was performed for relative quantification. The RT-PCR primer pairs used to detect splicing errors are listed in *SI Appendix*, Table S2.

Statistical Analysis. The statistical significance of differences between groups was analyzed using GraphPad Prism by performing the indicated statistical tests. Differences in the raw values among groups were considered statistically significant when $P < 0.05$. P values are denoted by $*P < 0.05$; $**P < 0.01$; $***P < 0.001$; NS, not significant with $P > 0.05$.

Data Availability. RNA-seq data have been deposited in the National Center for Biotechnology Information (NCBI) Sequence Read Archive (accession SRP274576). The mouse strains carrying the *Rnps1 unbalanced* and *F181I* alleles are available from the Mutant Mouse Regional Resource Center. All other data are included in the manuscript and/or supporting information.

ACKNOWLEDGMENTS. We thank Tao Wang (University of Texas Southwestern Medical Center) for helpful discussions about the analysis of splicing. This work was supported by NIH Grants AI125581 and AI100627 (B.B.) and by the Lyda Hill Foundation (B.B.).

Author affiliations: [a]Center for the Genetics of Host Defense, University of Texas Southwestern Medical Center, Dallas, TX 75390-8505; and [b]Department of Pharmaceutical Sciences, School of Pharmacy, University of Pittsburgh, Pittsburgh, PA 15261

1. Y. Shi, Mechanistic insights into precursor messenger RNA splicing by the spliceosome. *Nat. Rev. Mol. Cell Biol.* **18**, 655–670 (2017).
2. B. R. Graveley, Sorting out the complexity of SR protein functions. *RNA* **6**, 1197–1211 (2000).
3. G. Schmidt, D. Werner, Sequence of a complete murine cDNA reflecting an S phase-prevalent transcript encoding a protein with two types of nucleic acid binding motifs. *Biochim. Biophys. Acta* **1216**, 317–320 (1993).
4. A. Mayeda *et al.*, Purification and characterization of human RNPS1: A general activator of pre-mRNA splicing. *EMBO J.* **18**, 4560–4570 (1999).
5. C. Schwerk *et al.*, ASAP, a novel protein complex involved in RNA processing and apoptosis. *Mol. Cell. Biol.* **23**, 2981–2990 (2003).
6. A. G. Murachelli, J. Ebert, C. Basquin, H. Le Hir, E. Conti, The structure of the ASAP core complex reveals the existence of a Pinin-containing PSAP complex. *Nat. Struct. Mol. Biol.* **19**, 378–386 (2012).
7. L. Michelle *et al.*, Proteins associated with the exon junction complex also control the alternative splicing of apoptotic regulators. *Mol. Cell. Biol.* **32**, 954–967 (2012).
8. B. Deka, K. K. Singh, Multifaceted regulation of gene expression by the apoptosis- and splicing-associated protein complex and its components. *Int. J. Biol. Sci.* **13**, 545–560 (2017).
9. V. Boehm *et al.*, Exon junction complexes suppress spurious splice sites to safeguard transcriptome integrity. *Mol. Cell* **72**, 482–495.e7 (2018).
10. P. Wang, P. J. Lou, S. Leu, P. Ouyang, Modulation of alternative pre-mRNA splicing in vivo by pinin. *Biochem. Biophys. Res. Commun.* **294**, 448–455 (2002).
11. K. Fukumura, K. Inoue, A. Mayeda, Splicing activator RNPS1 suppresses errors in pre-mRNA splicing: A key factor for mRNA quality control. *Biochem. Biophys. Res. Commun.* **496**, 921–926 (2018).
12. H. Le Hir, D. Gatfield, E. Izaurralde, M. J. Moore, The exon-exon junction complex provides a binding platform for factors involved in mRNA export and nonsense-mediated mRNA decay. *EMBO J.* **20**, 4987–4997 (2001).
13. J. Lykke-Andersen, M. D. Shu, J. A. Steitz, Communication of the position of exon-exon junctions to the mRNA surveillance machinery by the protein RNPS1. *Science* **293**, 1836–1839 (2001).
14. T. Wang *et al.*, Real-time resolution of point mutations that cause phenovariance in mice. *Proc. Natl. Acad. Sci. U.S.A.* **112**, E440–E449 (2015).
15. P. Rangamani, L. Sirovich, Survival and apoptotic pathways initiated by TNF-alpha: Modeling and predictions. *Biotechnol. Bioeng.* **97**, 1216–1229 (2007).
16. S. Gupta, A decision between life and death during TNF-alpha-induced signaling. *J. Clin. Immunol.* **22**, 185–194 (2002).
17. R. M. Tavares *et al.*, The ubiquitin modifying enzyme A20 restricts B cell survival and prevents autoimmunity. *Immunity* **33**, 181–191 (2010).
18. J. Clark, P. Vagenas, M. Panesar, A. P. Cope, What does tumour necrosis factor excess do to the immune system long term? *Ann. Rheum. Dis.* **64** (suppl. 4), iv70–iv76 (2005).
19. M. Croft, The role of TNF superfamily members in T-cell function and diseases. *Nat. Rev. Immunol.* **9**, 271–285 (2009).
20. B. B. Aggarwal, Signalling pathways of the TNF superfamily: A double-edged sword. *Nat. Rev. Immunol.* **3**, 745–756 (2003).
21. G. Buchwald *et al.*, Insights into the recruitment of the NMD machinery from the crystal structure of a core EJC-UPF3b complex. *Proc. Natl. Acad. Sci. U.S.A.* **107**, 10050–10055 (2010).
22. V. I. Rebel *et al.*, Essential role for the p55 tumor necrosis factor receptor in regulating hematopoiesis at a stem cell level. *J. Exp. Med.* **190**, 1493–1504 (1999).
23. M. Yamashita, E. Passegué, TNF-α coordinates hematopoietic stem cell survival and myeloid regeneration. *Cell Stem Cell* **25**, 357–372.e7 (2019).
24. D. Bryder *et al.*, Self-renewal of multipotent long-term repopulating hematopoietic stem cells is negatively regulated by Fas and tumor necrosis factor receptor activation. *J. Exp. Med.* **194**, 941–952 (2001).
25. I. Dybedal, D. Bryder, A. Fossum, L. S. Rusten, S. E. Jacobsen, Tumor necrosis factor (TNF)-mediated activation of the p55 TNF receptor negatively regulates maintenance of cycling reconstituting human hematopoietic stem cells. *Blood* **98**, 1782–1791 (2001).
26. C. J. Pronk, O. P. Veiby, D. Bryder, S. E. Jacobsen, Tumor necrosis factor restricts hematopoietic stem cell activity in mice: Involvement of two distinct receptors. *J. Exp. Med.* **208**, 1563–1570 (2011).
27. J. C. Goldstein, N. J. Waterhouse, P. Juin, G. I. Evan, D. R. Green, The coordinate release of cytochrome c during apoptosis is rapid, complete and kinetically invariant. *Nat. Cell Biol.* **2**, 156–162 (2000).
28. S. Krishna, I. C. Low, S. Pervaiz, Regulation of mitochondrial metabolism: Yet another facet in the biology of the oncoprotein Bcl-2. *Biochem. J.* **435**, 545–551 (2011).
29. E. Brotin *et al.*, Bcl-XL and MCL-1 constitute pertinent targets in ovarian carcinoma and their concomitant inhibition is sufficient to induce apoptosis. *Int. J. Cancer* **126**, 885–895 (2010).
30. X. Li, T. Niu, J. L. Manley, The RNA binding protein RNPS1 alleviates ASF/SF2 depletion-induced genomic instability. *RNA* **13**, 2108–2115 (2007).
31. A. K. Mankan *et al.*, Cytosolic RNA:DNA hybrids activate the cGAS-STING axis. *EMBO J.* **33**, 2937–2946 (2014).
32. J. T. Weinreb *et al.*, Excessive R-loops trigger an inflammatory cascade leading to increased HSPC production. *Dev. Cell* **56**, 627–640.e5 (2021).
33. T. Zhou, M. C. Kinney, L. M. Scott, S. S. Zinkel, V. I. Rebel, Revisiting the case for genetically engineered mouse models in human myelodysplastic syndrome research. *Blood* **126**, 1057–1068 (2015).
34. H. Dvinge, E. Kim, O. Abdel-Wahab, R. K. Bradley, RNA splicing factors as oncoproteins and tumour suppressors. *Nat. Rev. Cancer* **16**, 413–430 (2016).
35. L. Chen *et al.*, The augmented r-loop is a unifying mechanism for myelodysplastic syndromes induced by high-risk splicing factor mutations. *Mol. Cell* **69**, 412–425.e6 (2018).
36. H. D. Nguyen *et al.*, Spliceosome mutations induce r loop-associated sensitivity to atr inhibition in myelodysplastic syndromes. *Cancer Res.* **78**, 5363–5374 (2018).
37. M. Kitagawa *et al.*, Overexpression of tumor necrosis factor (TNF)-alpha and interferon (IFN)-gamma by bone marrow cells from patients with myelodysplastic syndromes. *Leukemia* **11**, 2049–2054 (1997).
38. L. Molnár, T. Berki, A. Hussain, P. Németh, H. Losonczy, The role of TNF-alpha in myelodysplastic syndrome: Immunoserologic and immunohistochemical studies. *Orv. Hetil.* **141**, 1807–1811 (2000).
39. L. Molnár, T. Berki, A. Hussain, P. Németh, H. Losonczy, Detection of TNFalpha expression in the bone marrow and determination of TNFalpha production of peripheral blood mononuclear cells in myelodysplastic syndrome. *Pathol. Oncol. Res.* **6**, 18–23 (2000).
40. G. E. Verhoef *et al.*, Measurement of serum cytokine levels in patients with myelodysplastic syndromes. *Leukemia* **6**, 1268–1272 (1992).
41. G. Stifter, S. Heiss, G. Gastl, A. Tzankov, R. Stauder, Over-expression of tumor necrosis factor-alpha in bone marrow biopsies from patients with myelodysplastic syndromes: Relationship to anemia and prognosis. *Eur. J. Haematol.* **75**, 485–491 (2005).
42. C. N. Arnold *et al.*, A forward genetic screen reveals roles for Nfkbid, Zeb1, and Ruvbl2 in humoral immunity. *Proc. Natl. Acad. Sci. U.S.A.* **109**, 12286–12293 (2012).
43. X. Zhong *et al.*, Genetic and structural studies of RABL3 reveal an essential role in lymphoid development and function. *Proc. Natl. Acad. Sci. U.S.A.* **117**, 8563–8572 (2020).
44. Y. Kong, M. Karplus, Signaling pathways of PDZ2 domain: A molecular dynamics interaction correlation analysis. *Proteins* **74**, 145–154 (2009).
45. B. Webb, A. Sali, Comparative protein structure modeling using MODELLER. *Curr. Protoc. Bioinformatics* **54**, 5.6.1–5.6.37 (2016).
46. M. Y. Shen, A. Sali, Statistical potential for assessment and prediction of protein structures. *Protein Sci.* **15**, 2507–2524 (2006).
47. J. Wang, T. Hou, Develop and test a solvent accessible surface area-based model in conformational entropy calculations. *J. Chem. Inf. Model.* **52**, 1199–1212 (2012).
48. E. Wang *et al.*, End-point binding free energy calculation with MM/PBSA and MM/GBSA: Strategies and applications in drug design. *Chem. Rev.* **119**, 9478–9508 (2019).
49. W. Huber *et al.*, Orchestrating high-throughput genomic analysis with Bioconductor. *Nat. Methods* **12**, 115–121 (2015).
50. E. Mancini, A. Rabinovich, J. Iserte, M. Yanovsky, A. Chernomoretz, *ASpli: Analysis of alternative splicing using RNA-Seq.* R package version 1.14.0. https://bioc.ism.ac.jp/packages/3.11/bioc/manuals/ASpli/man/ASpli.pdf. Accessed 16 October 2020.